

Simulation and Flight Experiment of a Quadrotor Using Disturbance Observer Based Control

Hoiho Jeong^{*1}, Seunghwan Jo^{†1}, Seungkeun Kim^{‡1}, Jinyoung Suk^{§1}, and Yung-Gyo Lee^{¶2}

¹Department of Aerospace Engineering, Chungnam National University, 99 Daehak-ro, Yuseong-gu, Daejeon 305-764, Korea

²Korea Aerospace Research Institute

ABSTRACT

This study constructs the realistic aerodynamic and wind database for a quadrotor and applies disturbance observer based control (DOBC). The wind-tunnel experiment measures six degree-of-freedom forces and moments in various combinations of wind velocity and wind directions - $90^\circ \sim 90^\circ$ angle of attack and $-45^\circ \sim 45^\circ$ sideslip. Computational fluid dynamics (CFD) at the urban field is applied to simulate a complex airfield environment in severe weather conditions. The simulator integrates a multidimensional lookup table to simulate different environments that include the location of a quadrotor, time, and the condition of wind. Then, the disturbance observer based controller is designed with the simplified longitudinal and lateral moment dynamics of the quadrotor to compensate the nominal controller based on conventional PID control. This study compares the performance of the disturbance observer based control with that of the PID controller through simulation and flight experiment.

1 INTRODUCTION

Quadrotor systems are susceptible to disturbance due to their trade-offs in mechanical simplicity compared to efficient aerodynamic design as well as the complexity of rotor systems. In particular, wind disturbance is an important issue for quadrotor safety and mission viability in the performance of complex urban terrain and bad weather condition. In this paper, a quadrotor aerodynamic database is constructed and a control strategy for omnidirectional disturbance is established by designing a disturbance observer. In a previous study on quadrotor modeling and simulation, quadrotor modeling was performed by calculating the thrust coefficient through motor specification and thrust measurements experiment [1, 2, 3]. However, these studies has limitations, it does not reflect the

dynamic characteristics of the whole region of the quadrotor and does not reflect the model characteristics for controlling the disturbance. Therefore, for the precise modeling of the quadrotor in the simulation environment, this study constructs a quadrotor aerodynamic database based on the wind tunnel test. The wind tunnel experiment using DJI MATRICE 100 was conducted by the Korea Aerospace Research Institute (KARI). The aerodynamic test was performed under varying wind speeds and measured with three components of forces and moments and rpm. For more accurate modeling, we used the DJI MATRICE 100 CAD modeling data and motion capture cameras to measure the mass moment of inertia uses. In this paper, numerical simulation consists of multi-dimensional lookup tables for aerodynamics data provided by the KARI. The datadase consists of interpolated for a wide range of aerodynamic data. In this study, to compensate the limit of the PID controller, the DOBC is designed along with the PID controller on the pitch and roll axis respectively. Disturbance observer is a technique of observing or estimating model uncertainties and their effects on the system. The disturbance observer based control allows estimation by filtering the data of uncertainty such as the external load of the motor, friction force, and wind gust to compensate for the disturbance. In this study, we analyzed the performance of DOBC using numerical simulation. In addition, performance analysis using a blower fan was applied to the quadrotor by applying the DOBC. Finally, the performance of the disturbance observer was verified by calculating the RMSE (Root Mean Square Error) using the flight data acquired through the waypoint flight test.

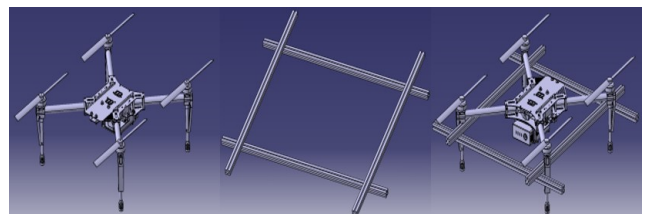


Figure 1: CAD modeling of DJI MATRICE 100 and apparatus.

*Email address(es): jeaonghoijo@cnu.ac.kr

†Email address(es): snipertype@cnu.ac.kr

‡Email address(es): skim78@cnu.ac.kr (corresponding author)

§Email address(es): jsuk@cnu.ac.kr

¶Email address(es): lyg@kari.re.kr

Table 1: DJI MATRICE 100 Specification.

Structure	
Diagonal wheelbase	650 mm
Weight	2355 g
Max takeoff weight	3600 g
Performance	
Max pitch angle	35 degree
Max speed of ascent	5 m/s
Max speed of descent	4 m/s
Max wind resistance	10 m/s
Max speed	17 m/s (no Wind)
Hovering time	22 min

2 DJI MATRICE 100 MODELING

2.1 Measurement of mass moment of inertia

A prior study of quadrotor modeling estimated the mass moment of inertia assuming a quadrotor's prop and fuselage as cylinders as shown in [4, 5]. However, this method is difficult to obtain accurate mass moment of inertia due to quadrotor geometry and mass distribution. Therefore, in this paper, mass moment of inertia were measured through data postprocessing using CAD design and motion capture camera. For accurate measurement of mass moment of inertia, fixtures were built and CAD models were designed with the same material and size as the DJI MATRICE 100. In addition, for measuring the mass moment of inertia on the roll, pitch, and yaw axis, four motion capture cameras were used to conduct a pendulum motion experiment for two minutes. The DJI MATRICE 100 model information provided by the DJI Corporation is shown in Table 1. Table 2 shows the DJI MATRICE 100 mass moment of inertia measured using a CAD design program. Roll and Pitch axis mass moment of inertia is around $0.05kgm^2$, and the Yaw axis is twice as large as the other axes. As shown in Table 3, because the cross-sectional area of the yaw axis is larger than that of the other axes, the area and weight distribution are larger than those of the other axes. For accurate experiment, DJI MATRICE 100 and fixtures were combined to measure mass moment of inertia. In order to construct the experimental environment using the motion capture camera, as shown in Figure 4, four OptiTrack motion capture cameras were installed at the corners of the cube profile structure and the camera focus was installed 60cm from the center of the ground. In order to record the movement of the object using the motion capture camera, the marker was attached to the center of the motor located at the end of each axis of DJI MATRICE 100, and a masking tape was attached to the top surface of the prop due to reflected light during data acquisition. To measure the mass moment of inertia, DJI MATRICE 100 was suspended from the ceiling by connecting KEVLAR yarns of the same length as shown

Table 2: Moment of inertia results measured by CAD.

Axis	DJI MATRICE 100 MOI	Apparatus MOI	DJI MATRICE 100 + Apparatus MOI	Unit
Roll	0.05535	0.05147	0.10682	kgm^2
Pitch	0.05784	0.06739	0.12523	
Yaw	0.10667	0.11854	0.22521	

in Figure 2. Experiments were performed for 3 times each for 2 minutes with different lengths of lines. At the same time, data acquisition and image capture of motion capture camera were performed at the same time. The mass moment of inertia is defined as a relational expression as shown in Eqs. 1-3 Figures 5 and 6 show two-dimensional graphs of data acquired for vertical and horizontal axis movements using a motion capture camera. The highest points in the pendulum motion are marked with a red marker to distinguish. Experimental results show that I_{zz} values are close to those calculated by CAD. The roll and pitch axis data using the motion capture camera shows a large error in each experimental case due to the problem of the experimental method. In this study, the mass moments of inertia calculated by CAD were determined to be equal to the model coefficients of the actual DJI MATRICE 100. Also, the roll and pitch axes are the same in consideration of the symmetrical shape of the quadrotor.

$$I_{xx} = \frac{W_1 T_1^2 L_1}{4\pi^2} - \frac{W_2 T_2^2 L_2}{4\pi^2} - \frac{W_3 L_3^2}{g} \quad (1)$$

$$I_{yy} = \frac{W_1 T_1^2 L_1}{4\pi^2} - \frac{W_2 T_2^2 L_2}{4\pi^2} - \frac{W_3 L_3^2}{g} \quad (2)$$

$$I_{zz} = \frac{W_1 T_1^2 A^2}{16\pi^2 L} - \frac{W_2 T_2^2 A^2}{16\pi^2 L} \quad (3)$$

2.2 Aerodynamic database

To construct a dynamics model, an aerodynamic database was constructed using the wind tunnel data of the DJI MATRICE 100 quadrotor performed by KARI. Equation 4 and 5 are the input and output formulas for building the quadrotor

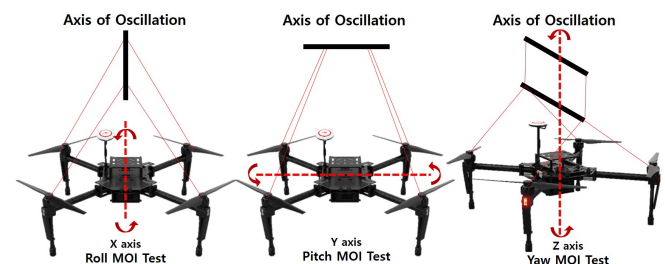


Figure 2: Roll, Pitch, Yaw MOI test axis

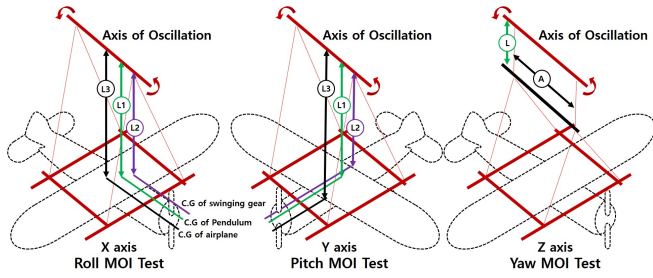


Figure 3: Measurement method of moment of inertia according to flight axis.

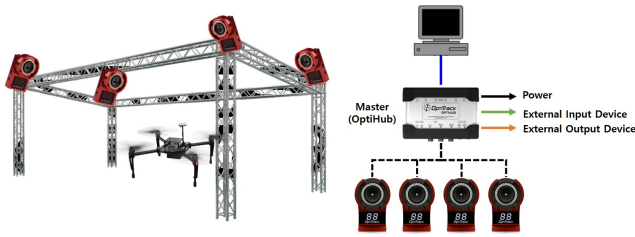


Figure 4: Motion capture camera environment configuration

aerodynamic database. The input variables constitute the Euler angles ϕ, θ, ψ and the body frame velocities U, V, W and RPM.

$$\begin{aligned} X_{body} &= Fn(\phi, \theta, \varphi, U, V, W, RPM, \delta RPM) \\ Y_{body} &= Fn(\phi, \theta, \varphi, U, V, W, RPM, \delta RPM) \\ Z_{body} &= Fn(\phi, \theta, \varphi, U, V, W, RPM, \delta RPM) \end{aligned} \quad (4)$$

$$\begin{aligned} L &= Fn(\phi, \theta, \varphi, U, V, W, RPM, \delta RPM) \\ M &= Fn(\phi, \theta, \varphi, U, V, W, RPM, \delta RPM) \\ N &= Fn(\phi, \theta, \varphi, U, V, W, RPM, \delta RPM) \end{aligned} \quad (5)$$

Because the motor input is different depending on the flight status, the motor RPM must be calculated based on the motor placement of the quadrotor as shown in Figure 7. In Figure 21, the aerodynamic database is constructed for the roll and pitch axes and is divided into blocks for each axis. The force and moment are calculated according to the motor command output. Each block receives the feedback of the

Table 3: DJI MATRICE 100 Sectional area.

Axis	Sectional area	Unit
Roll (Side)	0.0309	kgm^2
Pitch (Front)	0.0309	
Yaw (Top)	0.0848	

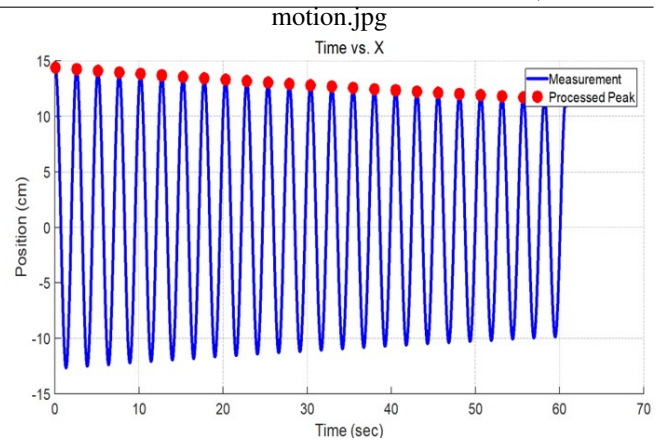


Figure 5: Peak value recording for directional axis pendulum motion

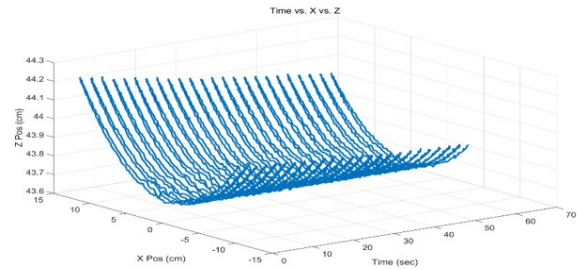


Figure 6: 3-Dimensional graph of transverse pendulum motion

state variables of the quadrotor, performs the calculation, and outputs the force and moment.

Figure 23 shows that the force and moment are constructed as a multi-dimensional lookup table according to the wind speed. The point outside the reference flight speed is calculated using interpolation. As a result, the aerodynamic database consists of a triple structure and the data for each axis is coupled. Therefore, the output results for each axis must be assigned to equations 6 and 7. Finally, the calculated force and moment are substituted into the quadrotor 6-DOF equation to yield the flight states.

$$\begin{aligned} X_{body} &= X_{\theta} + Y_{\phi} \\ Y_{body} &= Y_{\theta} - X_{\phi} \\ Z_{body} &= (Z_{\theta} + Z_{\phi})/2 \end{aligned} \quad (6)$$

$$\begin{aligned} L_{all} &= L_{\theta} + L_{\phi} \\ M_{all} &= M_{\theta} - M_{\phi} \\ N_{all} &= N_{\theta} + N_{\phi} \end{aligned} \quad (7)$$

3 BUILDING A SIMULATION ENVIRONMENT

3.1 Quadrotor Dynamics Model

Figure 8 shows the fixed coordinate system of the quadrotor. We set up the kinematic coordinate system considering

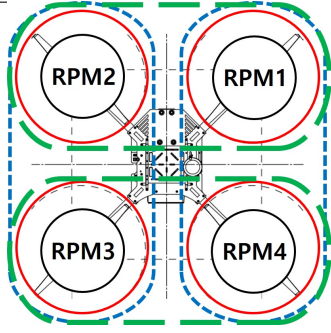


Figure 7: RPM coupling method

Table 4: Average Calculation based on RPM location.

Longitudinal RPM Average Calculation		Unit
Front RPM(1,2)	(RPM1+RPM2)/2	Ω
Rear RPM(3,4)	(RPM3+RPM4)/2	
Lateral RPM Average Calculation		Unit
Right RPM(1,4)	(RPM1+RPM4)/2	Ω
Lest RPM(2,3)	(RPM2+RPM3)/2	

DJI MATRICE 100 based on the X quadrotor frame. The state equations are defined as follows.

$$\begin{bmatrix} \dot{u} \\ \dot{v} \\ \dot{w} \end{bmatrix} = \begin{bmatrix} vr - wq + g \sin \theta \\ wp - ur - g \sin \phi \cos \theta \\ uq - vp - g \cos \phi \cos \theta \end{bmatrix} + \begin{bmatrix} X_{body} \\ Y_{body} \\ Z_{body} \end{bmatrix} / m \quad (8)$$

Here, the velocity state equation represents the acceleration on the center of mass of the quadrotor.

$$\begin{bmatrix} \dot{p} \\ \dot{q} \\ \dot{r} \end{bmatrix} = \begin{bmatrix} L/I_{xx} \\ M/I_{yy} \\ N/I_{zz} \end{bmatrix} - \begin{bmatrix} \frac{(I_{zz}-I_{yy})}{I_{xx}}qr \\ \frac{(I_{xx}-I_{zz})}{I_{yy}}pr \\ \frac{(I_{yy}-I_{xx})}{I_{zz}}pq \end{bmatrix} \quad (9)$$

The angular velocity state equation shows the roll, pitch and yaw changes taking into account the mass moment of

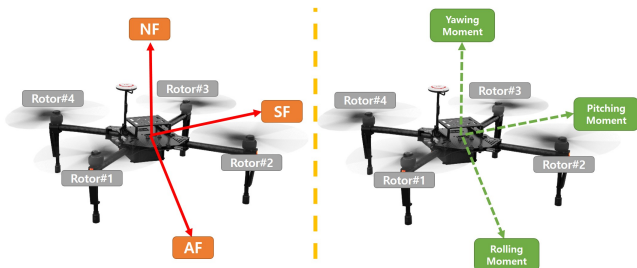


Figure 8: Quadrotor frame of reference

inertia, angular velocity and moment generated by the motor and the prop.

$$\begin{bmatrix} \dot{\phi} \\ \dot{\theta} \\ \dot{\psi} \end{bmatrix} = \begin{bmatrix} 1 & \tan \theta \sin \phi & \tan \theta \cos \phi \\ 0 & \cos \phi & -\sin \phi \\ 0 & \sin \phi / \cos \theta & \cos \phi / \cos \theta \end{bmatrix} \begin{bmatrix} p \\ q \\ r \end{bmatrix} \quad (10)$$

Equation 10 is the kinematics between the Euler angular rate and body rate.

3.2 Nominal Flight Controller

In general, the flight controller uses proportional, integral, and derivative control. The attitude controller provides the angle, position and angular velocity of the quadrotor to increase the safety of the quadrotor system by the P-PID structure. The altitude controller is based on a PID controller. The position controller is based on a PD controller.

$$\begin{aligned} \ddot{x} &= \{U_1(\cos \phi \sin \theta \cos \psi + \sin \phi \sin \psi) - K_1 \dot{x}\} / m \\ \ddot{y} &= \{U_1(\sin \phi \sin \theta \cos \psi - \cos \phi \sin \psi) - K_2 \dot{y}\} / m \\ \ddot{z} &= \{U_1(\cos \phi \cos \psi) - K_3 \dot{z}\} / m - g \end{aligned} \quad (11)$$

In equation 11, K_1 , K_2 and K_3 are the proportional gain in the attitude control loop.

$$\begin{aligned} u_1 &= \delta_{thr} = (+\Omega_1^2 + \Omega_2^2 + \Omega_3^2 + \Omega_4^2) \\ u_2 &= \delta_{ail} = (-\Omega_1^2 + \Omega_2^2 + \Omega_3^2 - \Omega_4^2) \\ u_3 &= \delta_{ele} = (-\Omega_1^2 - \Omega_2^2 + \Omega_3^2 + \Omega_4^2) \\ u_4 &= \delta_{rud} = (-\Omega_1^2 + \Omega_2^2 - \Omega_3^2 + \Omega_4^2) \end{aligned} \quad (12)$$

The control input is shown in equation 12 and means the RPM command for each motor. δ_{thr} , δ_{ail} , δ_{ele} and δ_{rud} are the virtual control input of the quadrotor by mixing the command values from the controller in Equation 12. u_1 , u_2 , u_3 and u_4 are the RPM.

Based on the X-shaped quadrotor shape as shown in Figure 8, the command is transmitted to the motor through the control mixing by the roll, pitch, yaw and altitude commands.

3.3 Disturbance Observer Based Control

Many controllers are designed based on the mathematical modeling of the system to be controlled [6, 7, 8]. Most controller are designed assuming no disturbance or are designed with worst-case assumptions. If disturbance exists, there is a possibility that the system becomes unstable because the nominal performance cannot be maintained and follow-up error occurs. There is a disadvantage in sacrificing desired control performance such as fast and accurate tracking performance in the absence of disturbance. However, most real-world systems do not fit mathematical modeling, and additional disturbances that are not taken into account from external environments are often applied to the system. These uncertainties can degrade controller performance and make

the system unstable. In this paper, we propose a robust control method that stabilizes the system and guarantees the control performance even in the presence of model uncertainty and disturbance. The DOBC (Disturbance Observer Based Control) was designed by combining with the PID controller. The DOBC is a technique for observing or estimating the effect of model uncertainty and disturbance on the system. It can be estimated by filtering data with uncertainties such as disturbance due to an external load of the motor, frictional force, gust and incomplete dynamics. The DOBC can compensate for these uncertainties. In addition, it can be designed by patching on the existing controller, and it is possible to guarantee the performance of the existing controller by compensating the disturbance. The DOBC depends on the design of the Q-filter, which is the nominal dynamics that the designer desires to model an uncertain system. There is a nominal performance restoration characteristic when there is no disturbance by deriving an additional control input in case of disturbance. And the controller technique provides robustness and adaptability. The DOBC block is shown in Figure 9. $C(s)$ has a basic PID structure as shown in equation 13.

$$C(s) = K_P + \frac{K_I}{s} + \frac{K_D s}{T_f s + 1} \quad (13)$$

Here, the PID controller is created through MATLAB Simulink, and T_f is set to 1 at this study. The disturbance observer is the key to the estimation input given to the real model and the inverse model. Knowing the exact $P(s)$ is difficult, the nominal model $P_n(s)$ can be obtained. Therefore, if the output of the model and the control input are given, we estimate the disturbance so that the DOBC compensates it. The Q-filters filters the noise and makes a proper transfer function of $P_n(s)^{-1}$. The control input shown in the DOBC structure can be expressed as in equation 14

$$u = \bar{u} + (y_p - \hat{u}_p) = \bar{u} - \hat{d} \quad (14)$$

$$u = \bar{u} + u_{filtered} - \frac{1}{J_{xx}} \dot{x}_{2,filtered} = \bar{u} + y_p - \hat{u}_p \quad (15)$$

Where \bar{u} is a nominal control input from the PID controller. The difference between the filter control input y_2 and the control input \hat{u}_2 , which includes the effect of the disturbance estimated through the inverse nominal model. Nominal model equation and attitude transfer function are represented in equations 16 - 17. Equation 18 shows the nominal model transfer function about roll control.

$$L = J_{xx} \ddot{\phi} \quad (16)$$

$$L = c_t \delta_{ail} - (J_{zz} - J_{yy}) \dot{\theta} \dot{\psi} \quad (17)$$

$$P_n(s) = \frac{\phi(s)}{\delta_{ail}(s)} = \frac{1}{J_{xx} s^2} \quad (18)$$

The Q-filter plays an important role in the DOBC for robust state and estimate disturbance. Q-filter should be designed to have at least the same relative order of nominal dynamics as shown in Equation 19.

$$Q_A(s) = Q_B(s) = \frac{a_0/\tau^2}{s^2 + (a_1/\tau)s + (a_0/\tau^2)} \quad (19)$$

Among the filter parameters, λ determines the accuracy of the disturbance estimation as an adjustable parameter. The smaller the λ , the better the transient response state, but the system may become unstable. The advantage of the DOBC is that it works only in disturbance situations and provides active anti-disturbance control with adaptability and robustness.

4 NUMERICAL SIMULATION

Comparing the case with and without the DOBC, the attitude and position tracking performance were analyzed by calculating RMSE (Root Mean Square Error).

$$\begin{aligned} \dot{p}_{dist} &= 7 \cos(t) \text{ (rad/s}^2\text{)} \\ \dot{q}_{dist} &= 7 \cos(t) \text{ (rad/s}^2\text{)} \\ \dot{r}_{dist} &= 5 \cos(t) \text{ (rad/s}^2\text{)} \end{aligned} \quad (20)$$

In Equation 20, the disturbance is applied to the pitch, roll, and yaw axes and multiplied by the mass moment of inertia to affect the moment equation. Figure 10 shows the simulation result using the PID controller. The X position cannot follow the position command after 40 seconds, and the Y position does not follow the command for the entire time domain. Figure 11 shows the result of the thrust command and

RPM using the PID controller. The thrust command shows slow response and the noise mixed in command.

Figure 12 shows the result of the simulation performed by combining the PID controller and the DOBC. Unlike the results by the PID controller, it can be seen that it follows the attitude and position command well. As shown in Figure 13, the RPM control also compensates for the disturbance estimated by the DOBC, while the noise is also reduced compared with the PID control while applying appropriate thrust command.

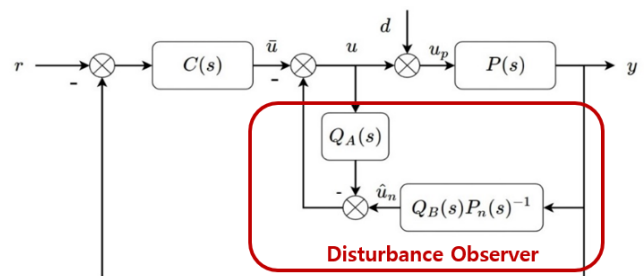


Figure 9: DOBC configuration

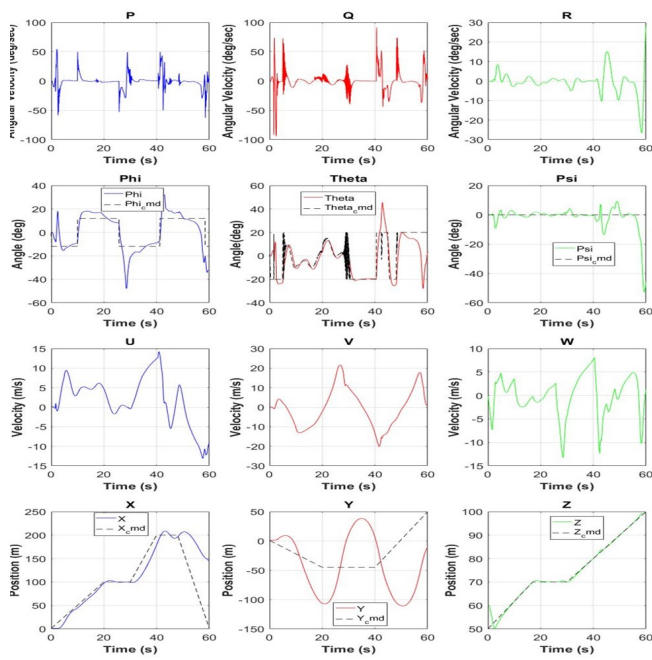


Figure 10: Simulation result - states (PID Controller).

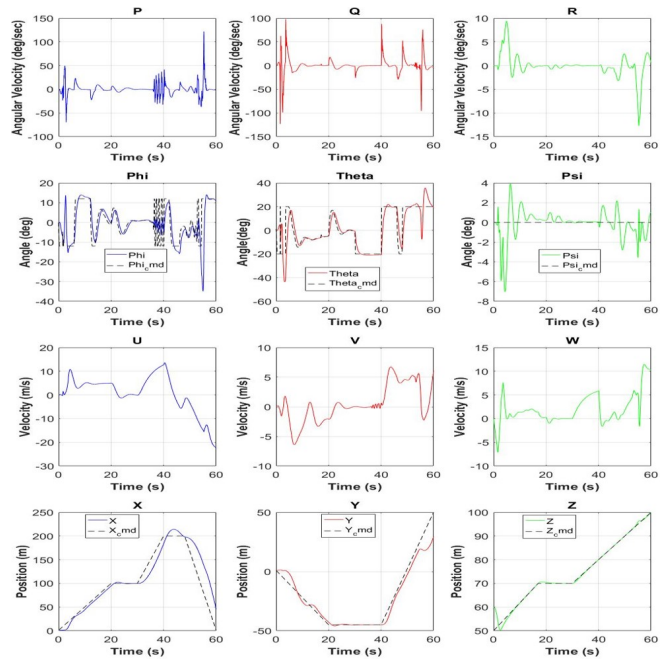


Figure 12: Simulation result - states (DOBC Controller).

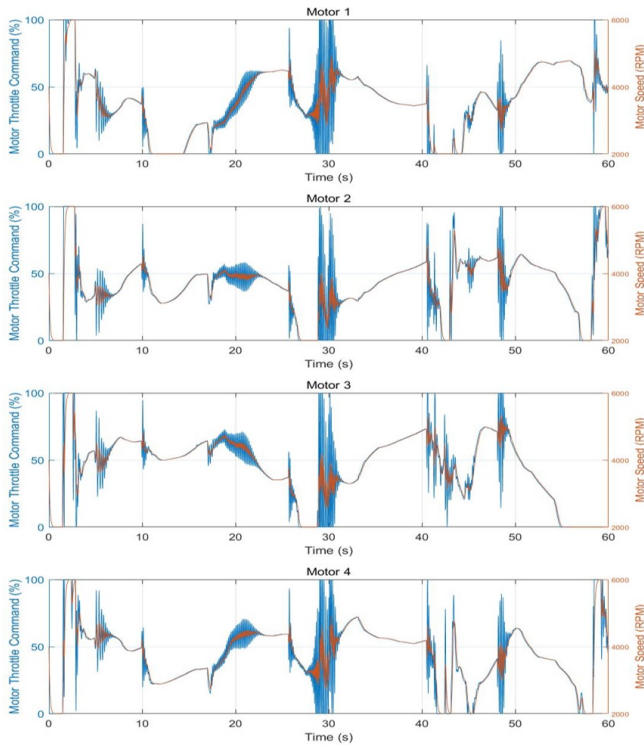


Figure 11: Simulation result - RPM (PID Controller).

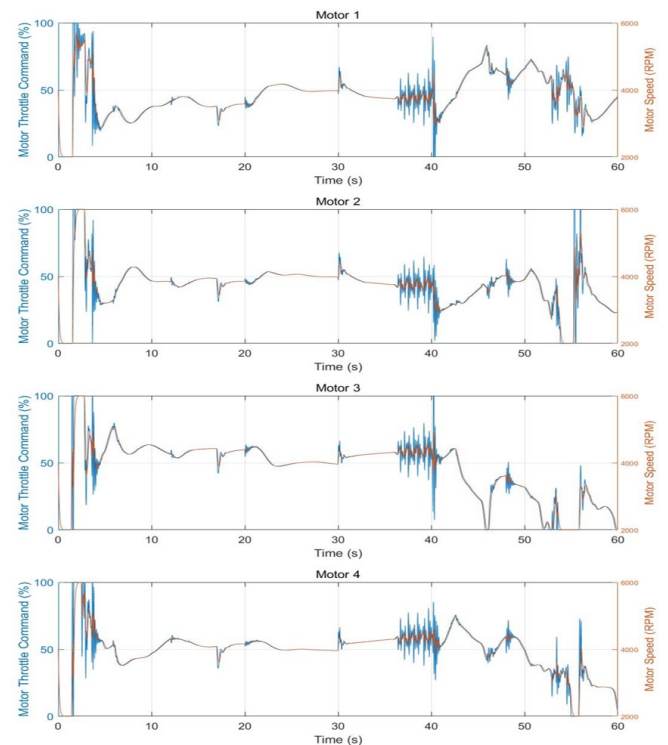


Figure 13: Simulation result - RPM (DOBC Controller).

Table 5: Simulation RMSE results comparison.

RMSE result (PID)		RMSE result (DOB)	
Phi (Degree)	0.1676	Phi (Degree)	0.1290
Theta (Degree)	0.1920	Theta (Degree)	0.1624
Psi (Degree)	0.2827	Psi (Degree)	0.1493
X (Position)	42.2538	X (Position)	24.2384
Y (Position)	64.4534	Y (Position)	6.2603
Z (Position)	1.3536	Z (Position)	1.3455

In order to numerically analyze the simulation results of the two control methods, the RMSE was calculated based on the simulation results. From the RMSE results, it can be seen that the simulation results using the DOBC against the attitude and position commands are improved than those using only the PID controller. The main tuning parameters of the DOBC were obtained numerically. The flight test was performed based on the DOBC variables obtained from the simulation.

5 FLIGHT TEST

5.1 Manufactured Quadrotor

The UASG-DOBC-Quadrotor shown in Figure 14 was developed so that aerodynamic modeling based on the aerodynamic data measured through the open wind tunnel experiment and aerodynamic characteristics is similar to the actual quadrotor. The FCC (Flight Control Computer) equipped in the UASG-DOBC-Quadrotor is Pixhawk Cube and the firmware is Ardupilot. The DOBC was combined with the PID - based attitude controller implemented in Ardupilot. We implemented the function to enable the DOBC according to the pilot command on the ground. The main control parameters of the DOBC were remotely modifiable in GCS (Ground Control System).

5.2 Performance Measurement Experiment of a Blower Fan

A blower fan produces disturbance environment. When flight tests are performed indoors, GPS accuracy drops.



Figure 14: UASG-DOBC-Quadrotor.

Therefore, the experimental environment was constructed as shown in Figure 15. The blower fan performance test was carried out using the climate measurement equipment to confirm the exact wind speed performance according to the distance. The measurement results are shown in Figure 16. The maximum wind speed was measured to be $14.6m/s$ and the wind speed decreased at a constant interval as the distance increased. In this study, the quadrotor will enter the disturbance path at a distance of about 2m from the blower fan, and then the attitude and position response of the quadrotor will be checked according to the control method.

5.3 Flight Test

In order to verify the performance of the DOBC before the waypoint flight test, a control performance experiment was performed using a blower fan. The test method is shown in Figure 17. In order to simulate the disturbance environment, the horizontal and vertical winds were implemented. The design variables of the DOBC were tuned through this test. Among them, when the τ is greatly reduced, the quadrotor itself oscillates even though it is not affected by the disturbance. After tuning the DOBC, we carried out the flight test using the dummy weights and finally performed the waypoint flight. As shown in Figure 19, the flight test using the dummy weight was carried out in three ways. Figures 24-27 show the flight test results for Method 3 among the flight tests shown in Figure 19. The flight test was conducted by disturbing the quadrotor by a person on the ground when hovering at an altitude of 4 meters. In order to have a periodic disturbance in the quadrotor, a person on the ground periodically pulls the string strongly. Figure 26 and 27 show that the DOBC as a whole greatly reduces the noise and follows the command value. Here, we can see the structural limit of the quadrotor. It can be seen that the yaw axis control force is insufficient due to the disturbance generated on the roll and pitch axes. Therefore, it is necessary to increase the control force on the yaw axis by rotating the motor thrust vector direction of the quadrotor in a future study. Figures 28 are the flight path results from the waypoint flight. As shown in Figures 19, the

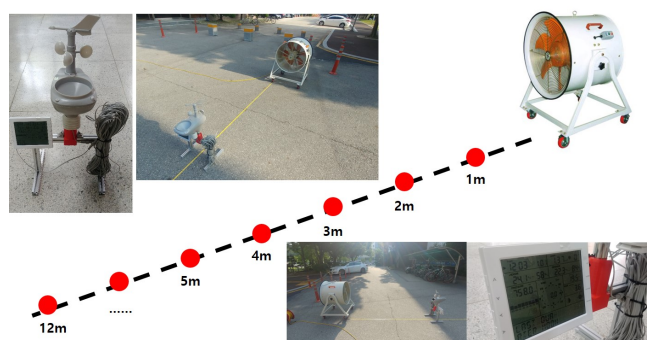


Figure 15: Performance measurement experiment of a portable blower fan.

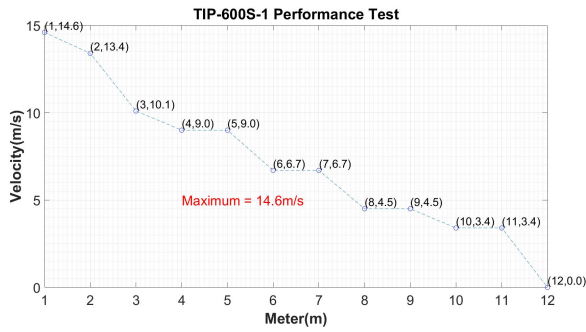


Figure 16: Blower fan performance test.



Figure 17: Flight test method using blower fan.

Table 6: Flight test RMSE results comparison

Contents	RMSE result (PID)	RMSE result (DOB)
Method 3 (Using Human Force) RMSE		
Phi rate (deg/sec)	0.3137	0.2570
Theta rate (deg/sec)	0.0659	0.0681
Yaw rate (deg/sec)	0.3076	0.3210
Phi (deg)	0.4245	0.2772
Theta (deg)	0.1013	0.1067
Yaw (deg)	0.5534	0.5032
Waypoint Flight Test RMSE		
Phi rate (deg/sec)	0.1069	0.1032
Theta rate (deg/sec)	0.1163	0.1094
Yaw rate (deg/sec)	0.3472	0.4499
Phi (deg)	0.1977	0.1882
Theta (deg)	0.2705	0.2408
Yaw (deg)	3.6156	3.5352

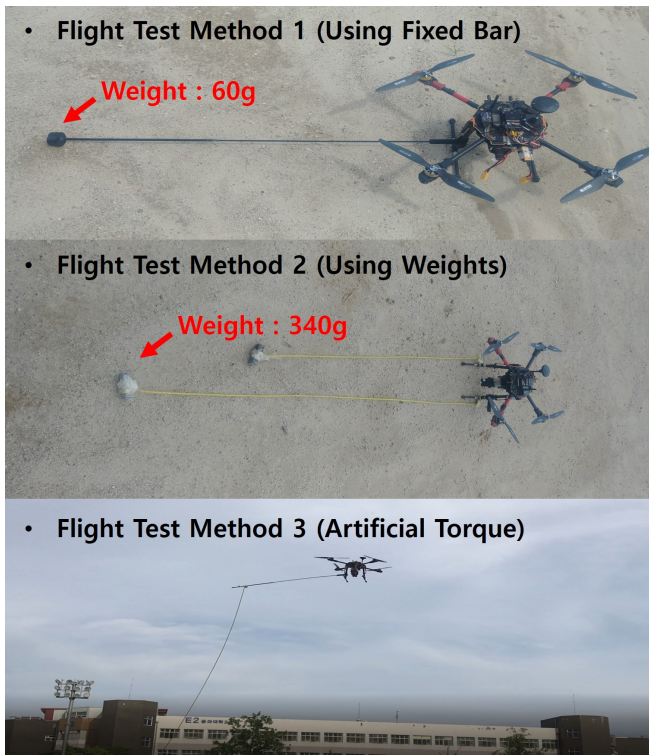


Figure 18: DOBC performance verification flight test method.

waypoint flight test was performed by attaching the weight to the quadrotor landing gear as shown in Method 2.

As the quadrotor moved, the weight tied to the line caused a moment in the quadrotor by pendulum movement in an unexpected direction. It can be seen that the DOBC follows the similar flight path by applying the DOBC even if the weight disturbance occurs. The RMSE (Root Mean Square Error) results for flight tests are shown in Table 6. From the angular velocity and Euler angle results, it can be seen that the error is smaller when the DOBC is applied. However, the lack of control yaw axis can be seen in waypoint flight test case. Therefore, future studies will improve this problem and proceed with the waypoint flight test.

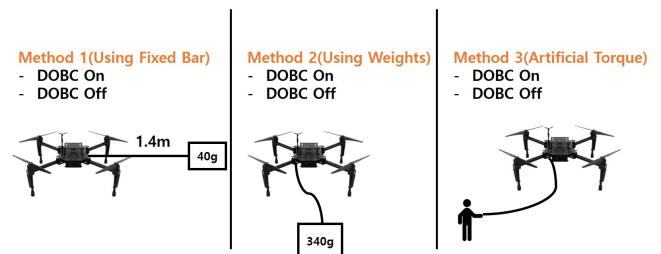


Figure 19: Flight test method with slung load uncertainty.



Figure 20: Waypoint flight path.

6 CONCLUSION

Simulation and flight tests manifested that the PID controller in disturbance environment has limitations and is impossible to keep robust control. In addition, when the DOBC was applied, it was possible to control the airframe by compensating the disturbance with uncertainty. The DOBC showed better performance in a strong disturbance environment. Such as slung load, artificial wind, and human interaction. Thus, the DOBC could effectively compensate the disturbance and increase flight stability of the quadrotor system. Future work DOBC will be done by patching on the position controller. And we propose a collision avoidance algorithm using DOBC using relative navigation and collision avoidance algorithm in a disturbance environment implemented in a room.

ACKNOWLEDGEMENTS

This work is supported by the research project (No. 10062497) funded by the Ministry of Trade, Industry and Energy of Korea, Republic of.

REFERENCES

- [1] S. Bouabdallah and R. Siegwart. Backstepping and sliding-mode techniques applied to an indoor micro quadrotor. In *IEEE International Conference on Robotics and Automation*, 2005.
- [2] M. Bouchoucha H. Bouadi and M. Tadjine. Sliding mode control based on backstepping approach for an uav type-quadrotor. *World Academy of Science Engineering and Technology*, 26(5):22–27, 2007.
- [3] A. M. Ashfaq and D. Wang. Modeling and backstepping-based nonlinear control strategy for a 6 dof quadrotor helicopter. *Chinese Journal of Aeronautics*, 21(3):261–268, 2008.
- [4] J. J. Lee. Experimental determination of mass moments of inertia for tilt rotor uav (unmanned aerial vehicle). In *The Korean Society for Aeronautical and Space Sciences Spring Conference*, 2013.
- [5] M. P. Miller. An accurate method of measuring the moments of inertia. In *NASA Reports, U.S., Report*, 1996.
- [6] S. K. Kim S. H. Jo, H. J. Jeaong and J. Y. Suk. Robust control of the small coaxial compound helicopter uav using disturbance observer based control. In *2017 Asia-Pacific International Symposium on Aerospace Technology*, 2017.
- [7] W. Ha K. Lee and J. Back. Overview of disturbance observation techniques for linear and nonlinear systems. *Journal of Institute of Control, Robotics and Systems (in Korean)*, 22(5):332–338, 2016.
- [8] S. H. Jeong and S. Jung. Design and experimental studies of a disturbance observer for attitude control of a quadrotor system. *Journal of Institute of Control, Robotics and Systems (in Korean)*, 19(11):1004–1010, 2013.

APPENDIX A: AERODYNAMIC MULTIDIMENSIONAL DATABASE

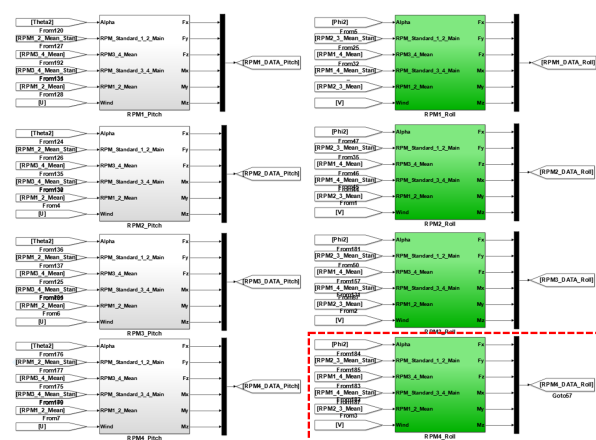


Figure 21: Aerodynamic database according to RPM number

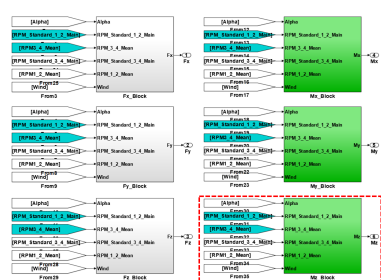


Figure 22: Force and moment aerodynamic database

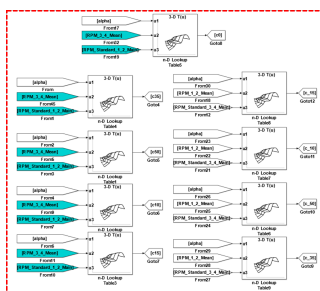


Figure 23: Aerodynamic database based on speed

APPENDIX B: FLIGHT TEST DATA

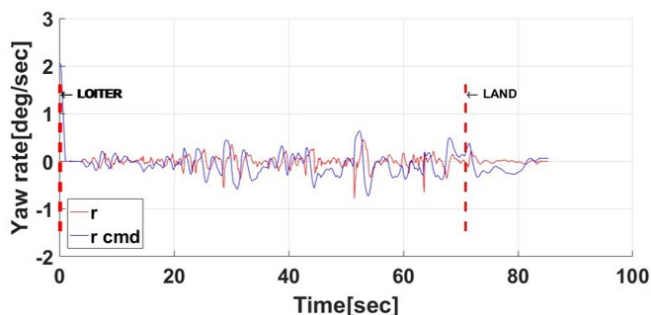
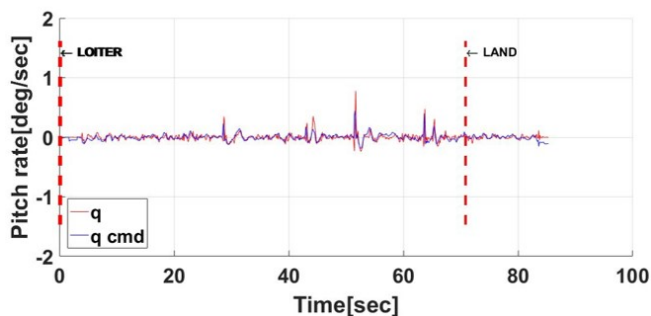
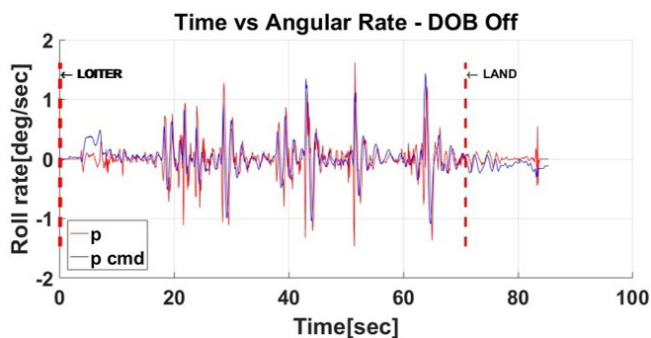


Figure 24: Method 3: Angular rate DOBC OFF.

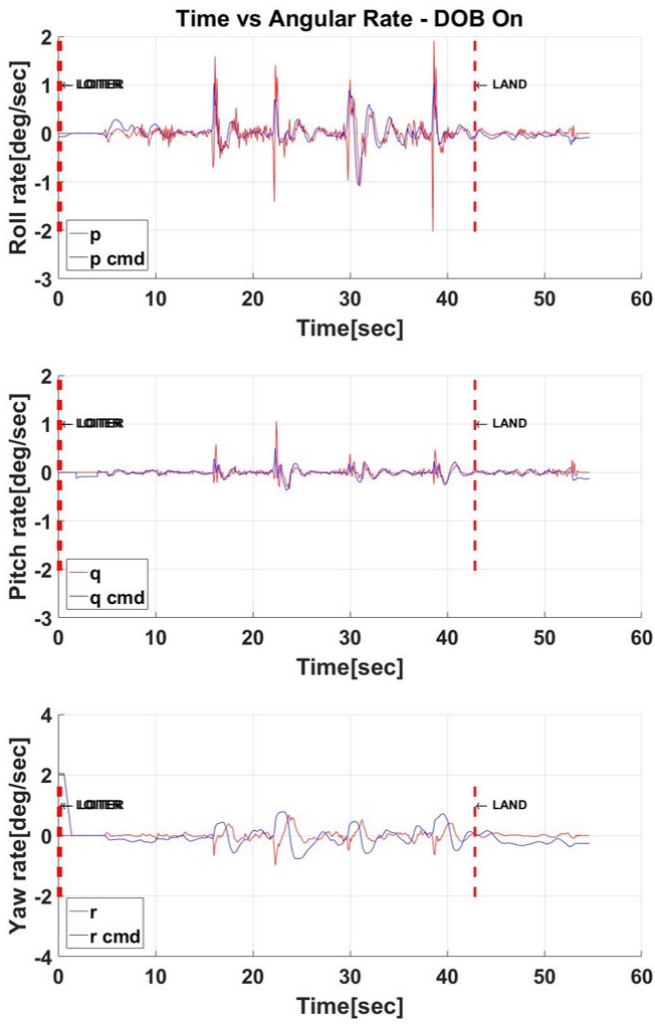


Figure 25: Method 3: Angular rate DOBC ON.

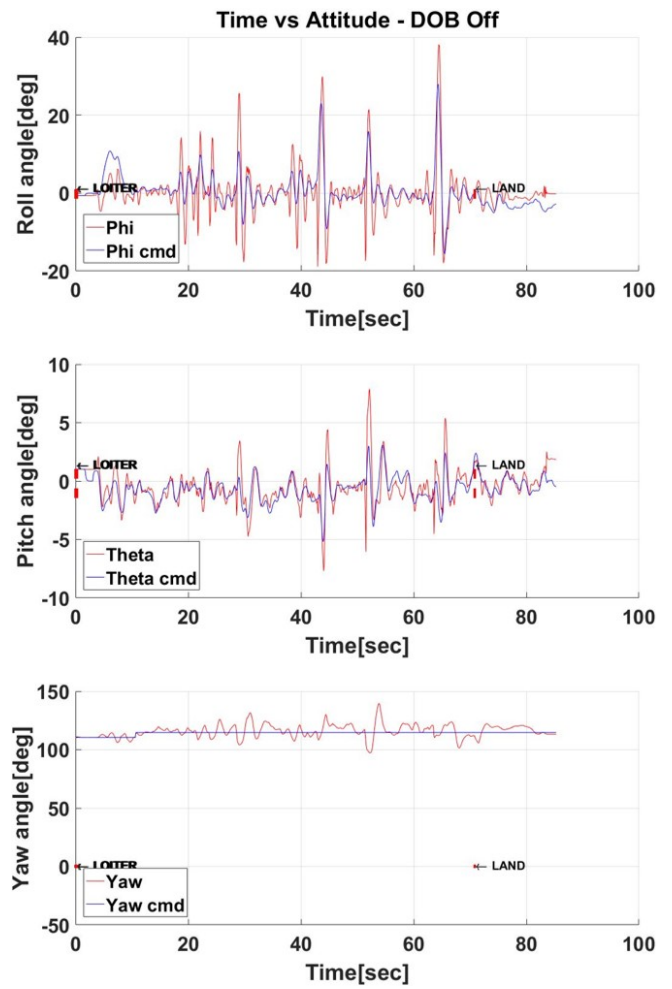


Figure 26: Method 3: Attitude DOBC OFF.

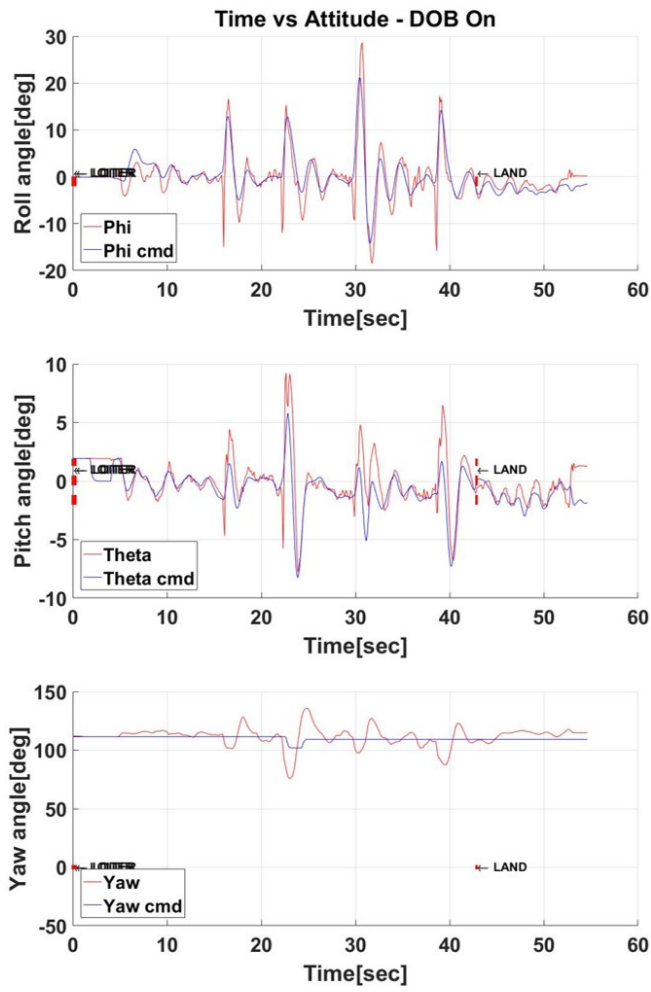


Figure 27: Method 3: Attitude DOBC ON.

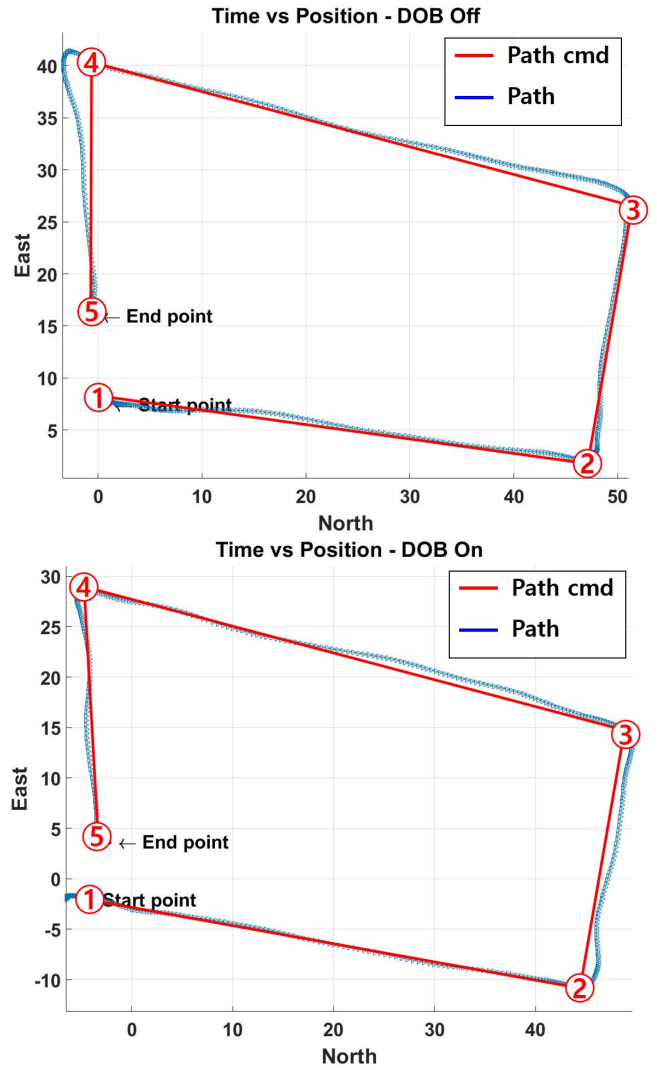


Figure 28: Waypoint flight: Path DOBC OFF / ON.